CHEMISTRY OF MATERIALS

ARTICLE

pubs.acs.org/cm

Structure Solution of the High-Pressure Phase of $CuWO_4$ and Evolution of the Jahn−Teller Distortion

J. Ruiz-Fuertes,*[,†] A. Friedrich,[‡] J. Pellicer-Porres,[†] D. Errandonea,[†] A. Segura,[†] W. Morgenroth,[‡] E. Haussühl,[‡] C.-Y. Tu,[§] and A. Polian[⊥]

[†]MALTA Consolider Team, Departamento de Física Aplicada-ICMUV, Universitat de València, Edificio de Investigación, c/Dr. Moliner 50, 46100 Burjassot, Spain.

[‡]Institut für Geowissenschaften, Abt. Kristallographie, Goethe-Universität Frankfurt, D-60438 Frankfurt am Main, Germany.

[§]Fujian Institute of Research on the Structure of Matter, Chinese Academy of Sciences, Fuzhou, Fujian 350002, China.

[⊥]Institut de Minéralogie et de Physique des Milieux Condensés, Université Pierre et Marie Curie-Paris 6, CNRS UMR 7590, 4 Place Jussieu, F-75252 Paris, France

Supporting Information

ABSTRACT: In this work, we have investigated the structural behavior of cuproscheelite up to 33.9 GPa by means of high-pressure single-crystal X-ray diffraction (SXRD) and extended X-ray absorption fine structure (EXAFS). According to EXAFS, beyond 9 GPa a phase transition takes place. On the basis of SXRD, the transition is from the triclinic ($P\bar{1}$) structure to a monoclinic ($P2/c$) structure isotypic to wolframite. The transition implies abrupt changes of CuO_6 and WO_6 octahedra, but no coordination change. Further, we report the role played by the Jahn−Teller distortion of the CuO_6 octahedra on the mechanism of the phase transition as well as the changes in the behavior of the Cu−O bonds for the triclinic and monoclinic phases of $CuWO_4$. A second phase transition was detected at 22.5 GPa. Finally, a low-temperature experiment has been carried out at 100 K. No structural changes were detected for $CuWO_4$, confirming the already known triclinic structure stability at room pressure and low temperature.

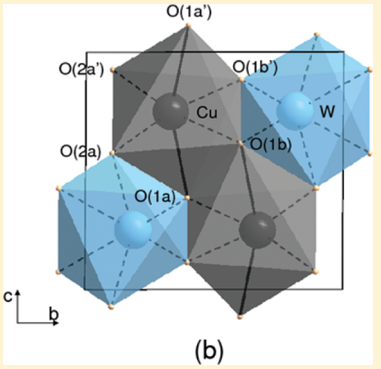

KEYWORDS: high-pressure, X-ray diffraction, EXAFS, phase transition, Jahn−Teller

1. INTRODUCTION

Tungstates of 3d-transition metals form an important family of inorganic materials with a high-application potential in various fields. These compounds are well-known as semiconductors with technological applications in scintillator detectors, laser hosts, photoanodes, optical guides,[1,2] etc. In particular $CuWO_4$ (cuproscheelite) has attracted interest as electrode for rechargeable Li batteries.[3] Moreover, in the last years, it has also attracted increased attention as a multiferroic material with an intriguing magnetic phase diagram.[4] $CuWO_4$ has been extensively studied at ambient pressure to characterize its optical,[5] transport,[6] magnetic,[4,7] and structural properties.[8] It crystallizes in a triclinic structure and can be described as a hexagonal close packing of anions, with the cations occupying half of the octahedral sites.[8] In earlier studies, the influence of the strong Jahn−Teller (JT) distortion of the CuO_6 octahedra on the physical properties of $CuWO_4$ has been discussed.[9,10] In particular, the JT effect gives rise to a reduction of the crystal symmetry, from $P2/c$ (the structure of wolframite-type oxides like $NiWO_4$ and $ZnWO_4$) to $P\bar{1}$.[8] In a previous work,[10] after powder X-ray diffraction and Raman spectroscopy measurements, a phase transition to a wolframite-type structure was found in $CuWO_4$ under compression at 10 GPa. Based upon *ab initio* calculations and optical absorption measurements[9,10] an almost complete quenching of the JT distortion was argued to happen at the phase transition. However, previous studies were not able to fully solve the crystalline structure of the high-pressure (HP) phase and only a Le Bail refinement attempt was made for the proposed monoclinic phase, giving us unit-cell parameters at 16.0(1) GPa: a = 4.52(5) Å, b = 5.53(6) Å, c = 4.89(5) Å, and β = 90.9(9)°. Moreover, a second phase transition was reported at 17.1(1) GPa.[10] The structure of the second HP phase is unknown yet. In addition, the equation of state of the low-pressure (LP) phase was found to depend upon the pressure-transmitting medium employed in the experiments.[10]

In this work, we have carried out single-crystal X-ray diffraction (SXRD) and extended X-ray absorption fine structure (EXAFS) studies under compression in order to solve the crystal structure of the HP phase of $CuWO_4$ and to better understand the HP phase transition process, putting the emphasis on the Cu local-structure behavior.

2. EXPERIMENTAL SECTION

Single-Crystal X-ray Diffraction at Ambient Conditions and 100 K. X-ray diffraction data were collected at 100 K and ambient

Received: June 6, 2011
Revised: August 9, 2011
Published: August 31, 2011

conditions, using an Xcalibur3 κ-circle diffractometer from Oxford diffraction with a charge-coupled device (CCD) camera and molybdenum (Mo) K_α radiation from a Mo anode operating at 45 kV and 38 mA. The Xcalibur3 instrument is equipped with a cryostream system (cryojet HT Oxford diffraction), stabilizing the sample temperature within ± 2 K. A single crystal with dimensions $80 \times 60 \times 40\ \mu m^3$ was used and mounted at a distance of 4.2 cm from the CCD. We collected 676 frames with a frame width of 0.75° and exposure time of 60 s in different settings of the diffractometer. Data reduction and empirical absorption corrections (Schwarzenbach) were performed using triclinic Laue symmetry by means of the program CRYSALIS.[11] We used as the starting atomic positions those obtained by Kihlborg and Gebert.[8] The structure refinements were carried out with SHELX97−2[12] and only the Cu and W atomic positions were refined with anisotropic displacement parameters, whereas O atoms were refined with isotropic ones.

Single-Crystal X-ray Diffraction at High Pressure. Two single-crystal X-ray diffraction experiments were performed under high pressure, one just below the onset of the phase transition at 7.0(1) GPa and the second one after the onset of the phase transition at 13.4(2) GPa to ensure that it had been already finished. Both intensity data collections were performed at beamline D3 at the HASYLAB synchrotron (Hamburg, Germany) using a HUBER four-circle diffractometer with Eulerian geometry, a NaI point detector (PD) and synchrotron X-ray radiation with a wavelength of 0.45 Å, provided by a Si(111) double-crystal monochromator. For the 7.0(1) GPa experiment we used an ETH-type diamond-anvil cell (DAC) with a tungsten gasket preindented to 90 μm with a 270 μm hole. In the pressure chamber, a single crystal ($93 \times 110 \times 30\ \mu m^3$) was loaded together with some ruby chips to measure the pressure. A methanol−ethanol mixture (4:1) was used as the pressure-transmitting medium. For the 13.4(2) GPa experiment a Boehler-Almax DAC[13] was used with a tungsten gasket preindented to 40 μm with a hole of 150 μm. A single crystal sample ($87 \times 67 \times 20\ \mu m^3$) was loaded with some ruby chips. Neon was used as pressure-transmitting medium in order to guarantee quasi-hydrostatic conditions.[14] All samples used were cut from the same large single crystal. In both experiments, the intensity data collection at HP was carried out with ω-scans. Diffractometer setting angles were set according to the fixed ϕ-technique,[15] in order to select the beam path of the least attenuation through the pressure cell. Intensity data were obtained from the scan data by the Lehmann-Larsen algorithm implemented in the beamline software REDUCE,[16] and corrected for Lorentz and polarization effects as well as for intensity drifts of the primary beam with AVSORT.[17] Finally, before carrying out the structural refinement with SHELX97−2,[12] all data were corrected for absorption both by the crystal as well as from the diamonds of the DAC by means of the ABSORB program in the version 6.0.[18] The starting parameters for the refinements were taken from ref 8 in the case of the 7.0(1) GPa experiment since no phase transition had occurred whereas for the 13.4(2) GPa experiment we used the SHELXS program implemented in SHELX97−2 to solve the structure. All the atomic positions were isotropically refined at both 7.0(1) and 13.4(2) GPa except for the W ones, which were refined anisotropically in the 13.4(2) GPa experiment.

Extended X-ray Absorption Fine Structure. XAS experiments were performed at the ODE beamline at the Soleil Synchrotron (Paris, France). ODE operates in the dispersive mode. A bent Si crystal is used to select the energy range of interest, containing the absorption edge under study (Cu K-edge, 8.980 keV) and to focus the beam down to a spot of $50 \times 40\ \mu m^2$. The whole spectrum was measured in one shot using a position sensitive detector. The energy scale was calibrated by measuring the spectrum of metallic Cu. High pressure was produced by means of a membrane diamond-anvil cell (MDAC).[19] The diamond anvils diffract the incident and transmitted beams giving rise to glitches in the spectrum. The MDAC must then be oriented in order to get rid of the glitches in the region of interest. The reference spectrum (I_0) used to calculate the absorption was measured outside the MDAC. Sample homogeneity is very critical when performing dispersive XAS measurements. In order to get a sample as homogeneous as possible we formed a 12 μm pellet (total absorption $\mu x \approx 1.6$) by compressing $CuWO_4$ powder (MaTeck) between both diamonds, which was then placed on the diamond surface, inside the 250 μm gasket hole. The remaining free space was filled with the pressure transmitting medium, silicone oil. Finally, we added a small ruby chip as a pressure sensor. Additionally, in order to improve the homogeneity of the sample thickness probed by the incoming X-ray radiation, the MDAC was shacked (10 μm amplitude) during the acquisition process.

3. RESULTS AND DISCUSSION

SXRD Analysis. The cuproscheelite structure is well-known since it was solved by Kihlborg and Gebert[8] in the late 60s by means of SXRD and compared in great extent to the wolframite family. As a reference for our structural studies at nonambient conditions and to confirm our crystal quality we carried out an SXRD experiment at ambient conditions and compared our results with those of Kihlborg and Gebert[8] (Table 1). The lattice parameters and the atomic positions obtained from our structure refinements are provided in Table 1, whereas all refinement details and atomic displacement parameters are found in the Supporting Information.

Ambient pressure and temperature experimental results match well with each other with small variations in the atomic positions (Table 1). We then investigated JT stability of the triclinic structure at low temperature by performing a SXRD experiment at 100 K. No transformation of the triclinic ($P\bar{1}$) structure was observed but only a volume compression of 0.6% (Table 1). In a previous structural study of this compound on powder samples, the stability of the triclinic structure was also reported in the high-temperature range from 353 to 1073 K.[20] Moreover, the triclinic structure was also found by Forsyth et al.[4] at 4 K. Summing up, we have added an additional volume versus temperature point to the temperature equation of state of triclinic $CuWO_4$. Hence, we can confirm, that there is no phase transition between 4 and 1073 K at ambient pressure. In addition, we have fit the previous[20] and present cell parameters as a function of temperature and obtained their thermal expansivity, $K_{a_i} = (1/a_i)(\partial a_i/\partial T)$, resulting in values of 8.6, 6.0, and 5.6 ($\times\ 10^{-6}\ K^{-1}$) for a, b, and c parameters, respectively. This is an interesting result because, as expected, those cell parameters that change most under compression[10] (a and b) are also those with the higher thermal expansivity.

To solve the HP structure as well as understand the transition mechanism we have carried out SXRD measurements on $CuWO_4$ under quasi-hydrostatic conditions. From a least-squares refinement of the positions of 22 centered reflections, we obtained accurate values for the lattice parameters of the triclinic structure at 7.0(1) GPa and of the HP structure at 13.4(2) GPa (Table 1).

The cell parameters at 7.0(1) GPa match well those obtained by means of powder XRD[10] at the same pressure with $a = 4.60(9)$ Å, $b = 5.72(11)$ Å, $c = 4.84(10)$ Å, $\alpha = 91.3(9)°$, $\beta = 91.5(9)°$, $\gamma = 84.3(9)°$. From the refinement of the crystal structure, we found that the JT distortion parameter, defined as[21] $\sigma_{JT} = (\sum_{i=1}^{6}(R_{Cu-O} - \langle R_{Cu-O}\rangle)^2)^{1/2}$ (where R_{Cu-O} are the six Cu−O distances of the CuO_6 octahedra and $\langle R_{Cu-O}\rangle$ is the

dx.doi.org/10.1021/cm201592h |Chem. Mater. 2011, 23, 4220–4226

Table 1. Cell Parameters and Wyckoff Positions of $CuWO_4$ at Different Pressure and Temperature Conditions

space group		$P\bar{1}$	$P\bar{1}$	$P\bar{1}$	$P\bar{1}$	$P2/c$
ref		ref 8	(this work)	(this work)	(this work)	(this work)
temperature (K)		293	293	100	293	293
pressure		1 atm	1 atm	1 atm	7.0(1) GPa	13.4(2) GPa
a (Å)		4.7026(6)	4.7080(10)	4.6950(10)	4.620(2)	4.542(6)
b (Å)		5.8389(7)	5.8400(10)	5.8320(10)	5.747(9)	5.461(16)
c (Å)		4.8784(6)	4.8840(10)	4.8760(10)	4.857(3)	4.980(9)
α (deg)		91.677(9)	91.77(3)	91.64(3)	91.34(10)	90
β (deg)		92.469(7)	92.47(3)	92.39(3)	91.48(5)	86.80(13)
γ (deg)		82.805(10)	82.81(3)	82.93(3)	84.69(9)	90
V (Å^3)		132.7(3)	133.1(3)	132.3(3)	128.3(3)	123.33(2)
Cu		2*i*	2*i*	2*i*	2*i*	2*f*
	x	0.49533(16)	0.4953(3)	0.4957(3)	0.4977(3)	0.5
	y	0.65976(13)	0.6601(3)	0.6596(3)	0.6619(8)	0.6701(13)
	z	0.24481(15)	0.2453(3)	0.2456(3)	0.2458(3)	0.25
W		2*i*	2*i*	2*i*	2*i*	2*e*
	x	0.02106(4)	0.02117(11)	0.02110(10)	0.01607(7)	0
	y	0.17348(3)	0.17347(9)	0.17346(8)	0.1769(2)	0.1867(4)
	z	0.25429(4)	0.2542(1)	0.25401(9)	0.25208(7)	0.25
O(1)		2*i*	2*i*	2*i*	2*i*	4*g*
	x	0.2491(10)	0.2489(2)	0.251(2)	0.2526(17)	0.253(2)
	y	0.3535(8)	0.3519(16)	0.3543(17)	0.358(4)	0.397(5)
	z	0.4245(10)	0.4239(19)	0.426(2)	0.4232(17)	0.3852(19)
O(2)		2*i*	2*i*	2*i*	2*i*	4*g*
	x	0.2145(10)	0.2162(19)	0.217(2)	0.2178(16)	0.2260(19)
	y	0.8812(7)	0.8811(16)	0.8825(17)	0.888(4)	0.897(5)
	z	0.4309(9)	0.4276(18)	0.431(2)	0.4306(16)	0.4263(19)
O(3)		2*i*	2*i*	2*i*	2*i*	
	x	0.7353(10)	0.7362(19)	0.734(2)	0.7388(17)	
	y	0.3803(8)	0.38013(16)	0.3803(16)	0.387(4)	
	z	0.0981(9)	0.0970(19)	0.096(2)	0.0941(17)	
O(4)		2*i*	2*i*	2*i*	2*i*	
	x	0.7826(9)	0.779(2)	0.783(2)	0.7763(15)	
	y	0.9079(8)	0.9073(17)	0.9075(17)	0.904(4)	
	z	0.0533(9)	0.0502(19)	0.053(2)	0.0613(15)	

average Cu−O distance), in the low-pressure phase is reduced upon compression from 0.48(1) Å at ambient pressure to 0.37(1) Å at 7.0(1) GPa. Hence, compression induces a 23% reduction of the CuO_6 JT distortion before the onset of the phase-transition.

The measurement of the unit-cell parameters at 13.4(2) GPa resulted in a monoclinic metric with a reduction in the *a* and *b* unit-cell parameters and an increase of the *c* axis. The obtained values slightly differ from those previously reported in ref 10 at 16.0(1) GPa and obtained with powder sample in silicone oil by means of a Le Bail refinement. This is probably due to the lower compressibility of $CuWO_4$ in less hydrostatic pressure media[10,22] (silicone oil is less hydrostatic than neon in the pressure range covered by our experiments[14]). According to ref 10, this fact is even more evident for the *a* and *b* cell parameters. This phenomenon together with the uncertainty induced by the broadening of Bragg reflections observed in ref 10 explains the differences in unit-cell parameters. An exploration of the systematic extinctions of the respective intensity data collection supported the monoclinic symmetry in Laue group $2/m$, with *b* being its unique axis, as only the ($h0l$: $l = 2n$) extinction rule applied. This extinction rule reduces the number of possible space group candidates to $P2/c$ or $P2_1/c$. From the data set collected, it was not possible to check whether the ($0k0$: $k = 2n$) extinction rule applies, as the crystal plate could only be cut parallel to the preferred exfoliation plane, which is the (010) plane for $CuWO_4$, and was placed in the DAC with this plane perpendicular to the rotation axis of the DAC. This prevented us from measuring the {$0k0$} Bragg reflections. A careful observation of the Cu and W atomic coordinates below the phase transition shows that the effect of pressure consists of moving both triclinic *x* and *z* coordinates to values closer to 0.5,*y*,0.25 and 0,*y*,0.25 for Cu and W, respectively. These special positions are finally occupied in the structure of the monoclinic HP phase. The magnitude of changes in the unit-cell parameters at the phase transition does not support large movements of the atoms through the phase transition, which makes the space group $P2_1/c$[23] as a candidate for the HP phase of $CuWO_4$ unlikely. The structure solution finally confirms space group $P2/c$ for the HP wolframite phase with residual values of R_1 = 3.09 and wR_2 = 6.67% for the refinement (see the Supporting Information).

dx.doi.org/10.1021/cm201592h |*Chem. Mater.* 2011, 23, 4220–4226

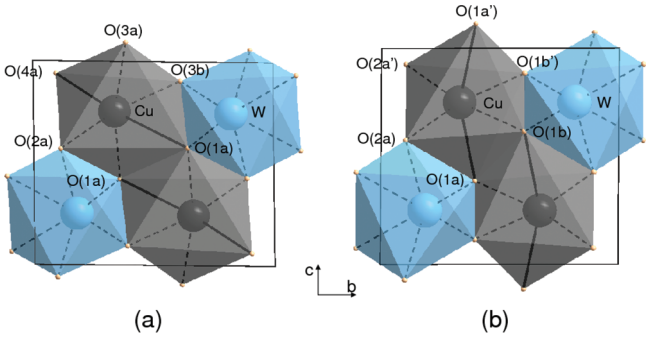

Figure 1. Crystal structure of $CuWO_4$ at (a) 7.0(1) and (b) 13.4(2) GPa. A shortening of the *a* and *b* axes as well as an elongation of the *c* axis due to a reorientation of the JT CuO_6 principal axis can be seen.

The monoclinic HP structure is compared with the triclinic structure in Figure 1. In order to facilitate the direct comparison of the oxygen atom positions of the two structures a setting with $\beta < 90°$ was chosen for the monoclinic $CuWO_4$ HP structure (Table 1). This relates to the further decrease in the β angle at the phase transition. According to the symmetry increase at the phase transition the oxygen atom positions of O(1) and O(3) as well as those of O(2) and O(4) of the low-pressure phase, are related via the *c*-glide plane in the HP phase leading to only two nonsymmetry equivalent oxygen positions (Table 1). We want to remark here that the nomenclature of the two oxygen atom positions measured for the monoclinic HP structure is vice versa to that commonly used in other monoclinic wolframites, e.g., in $MgWO_4$, as it was adapted to the nomenclature of triclinic $CuWO_4$ to facilitate comparison. Two features that can be directly appreciated in the HP structure are (i) the reduction in *a* and *b* unit-cell parameters as well as an increase in *c* and (ii) the maintenance of octahedral coordination for both Cu and W atoms. Thus, the structure of the HP phase can be described as isotypic to wolframite, with the difference that for $CuWO_4$ the CuO_6 distortion is larger than that of other monoclinic wolframites (see Table 2). For wolframite-type $CuWO_4$ we obtained $\sigma_{JT} = 0.32(4)$ Å at 13.4(2) GPa, a value larger than in wolframite-type $CdWO_4$ (0.22(2) Å). In HP $CuWO_4$, the orientation of the elongated axis of CuO_6 units is changed with respect to that in low-pressure $CuWO_4$. In Figure 1, a solid line highlights the elongated axis. In the triclinic structure, this axis is formed between marked atom O(4) and its opposite parallel to $[11\bar{1}]$; in wolframite, it is that formed between O(1) and the opposite oxygen, nearly oriented parallel to [101]. There are two possible hypotheses to explain this. The first one is that during the phase transition the CuO_6 octahedra are tilted. The second one is that the elongated axis is more compressed than the other two axes until the structure reaches a pressure of instability. At this pressure, the former elongated axis is collapsed and one of the short axes is elongated giving rise to the phase transition. The last hypothesis is the most probable since the oxygen atom positions are very similar in both structures. Thus, during the phase transition the atomic positions are only slightly moved and so the O(4) [O(3)] atom in the triclinic structure finds its equivalent in the O(2) [O(1)] atom of the monoclinic structure. This is also in accordance with the shortening of the *a* and *b* axes and the increase of the *c* axis with pressure. The results presented in the next section will provide us more information about the mechanism of this phase transition.

Table 2. Cu−O and W−O Distances (Å) of the CuO_6 and WO_6 Octahedra for the Refined Structures of $CuWO_4$ at Different Temperatures and Pressures

pressure	1 atm	1 atm	7.0(1) GPa	13.4(2) GPa	
temperature (K)	100	293	293	293	
Cu−O(2a)	1.96(1)	1.947(9)	1.963(16)	1.924(19)	Cu−O(2a)
Cu−O(1a)	1.95(1)	1.971(9)	1.954(8)	2.215(10)	Cu−O(1a)
Cu−O(3a)	1.97(1)	1.980(9)	1.985(9)	2.219(10)	Cu−O(1a′)
Cu−O(3b)	2.00(1)	2.004(9)	1.99(2)	1.96(2)	Cu−O(1b′)
Cu−O(4a)	2.34(1)	2.34(1)	2.202(16)	1.938(19)	Cu−O(2a′)
Cu−O(1b)	2.44(1)	2.46(1)	2.359(19)	1.97(2)	Cu−O(1b)
W−O(1b)	1.77(1)	1.753(9)	1.758(16)	1.781(19)	W−O(1b)
W−O(4b)	1.81(1)	1.81(1)	1.848(9)	1.914(11)	W−O(2b′)
W−O(3c)	1.85(1)	1.847(9)	1.842(17)	1.784(19)	W−O(1c′)
W−O(2b)	2.00(1)	2.009(9)	1.967(9)	1.921(12)	W−O(2b)
W−O(2c)	2.03(1)	2.026(9)	2.030(19)	2.11(2)	W−O(2c)
W−O(4c)	2.21(1)	2.23(1)	2.177(17)	2.10(2)	W−O(2c′)

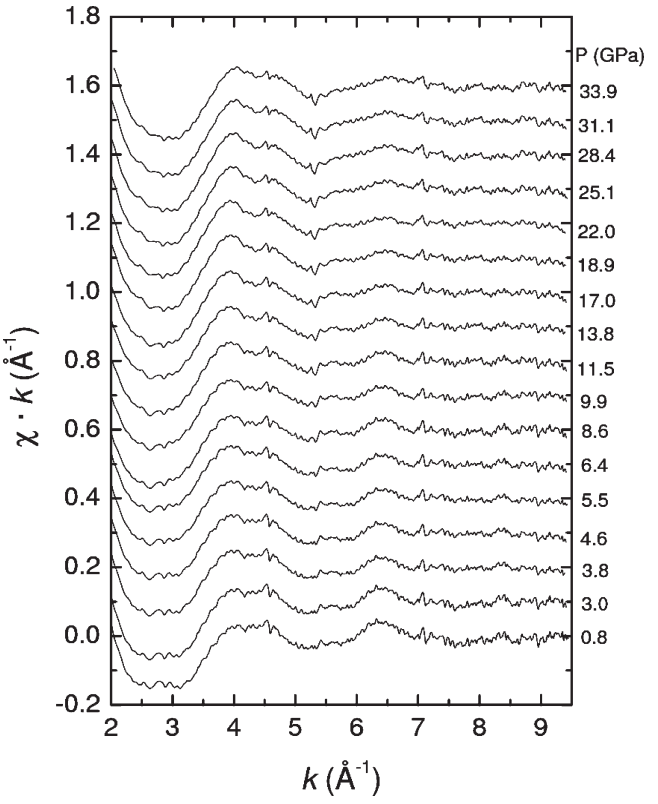

Figure 2. EXAFS signal at different pressures. For the analysis, we have used a *k* range from 2 to 7 $Å^{-1}$.

EXAFS Analysis. The EXAFS signals were extracted from the normalized spectra using a single cubic spline determined by least-squares approximation. The absorption-edge energy was set at the zero of the second derivative of the absorption spectra. No significant jump of E_0 was observed across the phase transition obtaining an E_0 of around 8.99 eV for all of them. The appearance of unavoidable glitches coming from the diamonds, as well as the presence of inhomogeneities on the absorption spectra set the high *k* limit. In Figure 2 the EXAFS signal at different pressures

dx.doi.org/10.1021/cm201592h |*Chem. Mater.* 2011, 23, 4220–4226

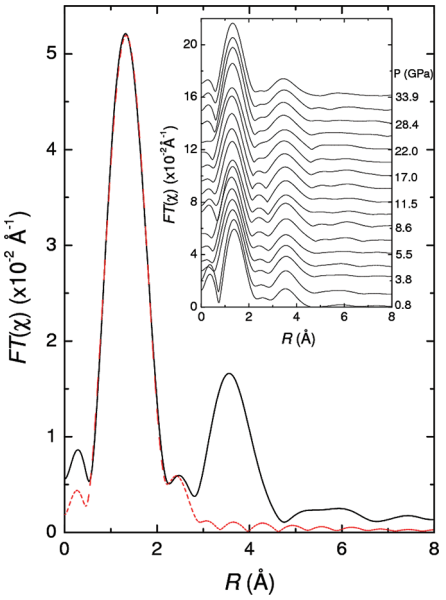

Figure 3. Pseudopair distribution function at 3.8(1) GPa obtained by the Fourier transformation (FT) of the EXAFS signal. The dotted red line represents the fit to the main peak. The inset graph summarizes the FT at the measured pressures.

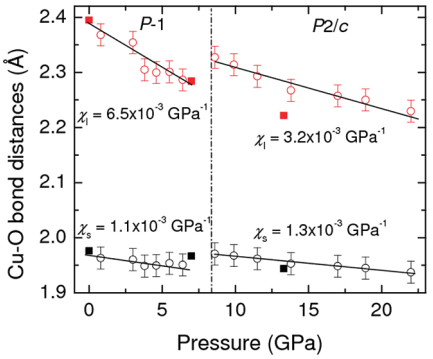

Figure 4. Evolution of the Cu−O distances with pressure. Empty circles represent the EXAFS data whereas the solid squares represent the SXRD results.

shows to be very stable in the presented k range (around 7 Å^{-1}), with a slight and progressive flattening of the signal as pressure increases. It is interesting to note that since at the first phase transition at 8.6(1) GPa there is no coordination change for Cu, the XANES portion of the absorption spectrum does not provide any further information and hence we will focus on the analysis of the EXAFS signal.

As we discussed above, in spite of the six different Cu−O bond distances, the CuO_6 units can be considered as elongated octahedra with four short and two longer bonds. An accurate determination of the six distances in powder samples by means of EXAFS is a challenging task, but trying to follow all of them under pressure (with the limited k-range of the DAC) is impossible. Therefore, to analyze the experiments we have assumed that CuO_6 octahedra are perfectly elongated units with only two Cu−O distances to follow: the elongated one (d_l), the average of the two longest distances, and the short one (d_s), the average of the remaining distances. Then the structural model of the Cu environment consists of two oxygen neighbor shells for Cu at d_l = 2.395 Å, and d_s = 1.976 Å, at ambient conditions. In the inset of Figure 3 we show the Fourier-transform peaks at different pressures obtained from the EXAFS spectra presented in Figure 2. A Bessel apodization window was used in the transformation.

In Figure 3, we can observe that both neighboring shells contribute to the same narrow and intense peak in the pseudopair distribution function that extends from 0.75 to 2.33 Å. On pressure increase the main peak moves toward lower R values, which points to a decrease of the Cu−O distances. However, it is interesting to note that discontinuities are observed by peak shifts back to higher distance values when the phase transitions take place. The spectra were fit with WinXas[24] and FEFF 8.2[25] was used to calculate the phases and amplitudes corresponding to both shells. A self-consistent calculation with a cluster of 128 atoms extending up to 4.1 Å from the absorbing atom was done. The amplitude reduction factor S_0^2 = 1.00 and the energy shift E_0 = −2.6 eV were deduced from the 3.8(1) GPa spectrum and then used for the fits of the other spectra. Once the S_0^2 and the E_0 parameters were deduced for the 3.8(1) GPa spectrum, only 4 free parameters were adjusted in each fit: both mean distances, as well as both pseudo-Debye−Waller factors σ_1^2 and σ_s^2. In Figure 3, the fit to the 3.8(1) GPa spectrum is plotted as the dotted line. The fits remain as good as this one up to 22.0(2) GPa when it worsens, probably due to the approach to the onset of the second phase transition.

In Figure 4, we show the pressure dependence of Cu−O bond distances obtained from SXRD (squares) and EXAFS (circles) for the first two phases. The agreement between the results of both experimental techniques is good from the experimental point of view. The 10% difference observed in the long Cu−O bonds in the HP phase at around 13.4(2) GPa could be caused by the use of a more hydrostatic medium in SXRD experiments in addition to the fact that for the SXRD measurements we used a single crystal, whereas powder samples were used for EXAFS. By using powder, we obtain an average in the Cu−O distances directly related to the coexistence of both LP and HP phases.[10] In addition, from the EXAFS data analysis point of view, the uncertainty in distance determination is increased by the use in the whole pressure range of the phases and amplitudes corresponding to the low pressure phase, which on the other hand is necessary in order to reliably establish the distance variations across the phase transition. Additional uncertainties are of course introduced in the fitting process as a result of describing a single peak in the pseudoradial distribution function with two shells. Moreover some uncertainty is introduced in the present SXRD experiment by the absence of any information on the {0k0} crystallographic plane because of experimental limitations.

The discontinuity in the bond distances is detected at a pressure similar to that of the previously reported phase transition, by means of crystal-field optical absorption spectroscopy,[9] to wolframite with a change being observed beyond 8.6(1) GPa. As expected with a technique that is very sensitive to local changes, with EXAFS the first transition is found 1 GPa below the previously reported transition pressure. The bond compressibility ($\chi = (-1/d)(\partial d/\partial P)$) obtained for every mean distance is also provided in Figure 4. As is expected, the compressibility of the longest distance is higher for the first two phases than that of the short distance. The effect of this difference, however, is not large enough to produce the disappearence of the JT distortion as can be seen in Figures 4 and 5. In the HP-wolframite phase, the reduction of σ_{JT} upon compression is lower than in the

dx.doi.org/10.1021/cm201592h |Chem. Mater. 2011, 23, 4220–4226

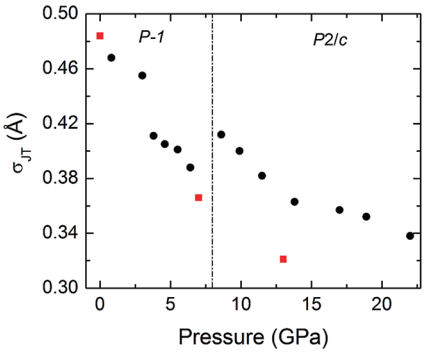

Figure 5. Pressure dependence of the JT distortion with pressure for the measured pressure range. Squares, SXRD; circles, EXAFS.

low-pressure triclinic structure given the smaller compressibility of the large Cu−O bonds (see Figure 4). Another striking result is that during the phase transition, both mean distances, the short and the long one, increase. This is unusual as a shortening of distances is expected on compression. In $CuWO_4$, however, the phase transition is ruled by the JT effect and so the observed increase in the Cu−O distances would be a consequence of the JT reaccommodation. This is reasonable because the JT distortion at around 9 GPa takes a value of 0.41 Å, according to EXAFS which is a value an order of magnitude larger than the increase of distances during the transition. The volume compression of $CuWO_4$ at pressure increase, hence, is assumed to be accommodated by the WO_6 octahedra or by changes of the inter- or intrapolyhedral angles. Unfortunately, this information cannot be extracted from the EXAFS data.

Regarding the phase transition mechanism, one possibility is the frustration of the JT quenching. The strong JT effect appears to be a competitor against the CuO_6 octahedral symmetry increase induced by pressure. Apparently at the pressure when σ_{JT} = 0.39(1) Å is reached, the triclinic structure becomes unstable and an abrupt alteration of the CuO_6 octahedra takes place reducing the former long axis and elongating one of the other axes. This new local structure produces an increase of the overall symmetry and the phase transition from the triclinic to the monoclinic phase occurs.

In Figure 3, a broadening of the pseudopair distribution function can be noticed beyond 25.1(2) GPa accompanied by an intensity increase. This fact together with a worsening of the fit quality by means of the model (2 + 4 distances) can be interpreted as a second phase transition that happens around 22.5(2) GPa. This is consistent with the second transition observed in PXRD experiments[10] performed using silicone oil as pressure transmitting medium as well. The overestimation of the second-transition pressure could be related to slight differences in the pressure environment of the sample as well as the influence of possible coexistence of phases. For this third phase, an attempt to make a fitting has been made with two different models considering a Cu coordination of two plus four Cu−O distances as well as three plus three ones but without success. Because the structure of the second high-pressure phase remains to be solved and the phase transition takes place at a pressure where silicone oil is far from hydrostatic, we have decided not to include those results in Figure 4.

4. CONCLUSIONS

By means of SXRD, we have solved and refined the HP structure of $CuWO_4$ at 13.4(2) GPa finding it isotypic to wolframite; however, the JT distortion of the CuO_6 octahedra is not suppressed. To fully understand the transition mechanism the structure has also been refined below the phase transition at 7.0(1) GPa. Moreover, we have performed EXAFS experiments in the Cu K-edge up to 33.9(3) GPa, determined Cu−O distances as a function of pressure for the different $CuWO_4$ phases, and compared them with the SXRD results. These measurements confirm the existence of a second transition at 22.5(2) GPa when experimental conditions are not fully hydrostatic. We have proposed that the transition is related to the limit of the reduction of the JT distortion of CuO_6 octahedra. Finally, by means of a low-temperature measurement we have added another point to the already studied temperature range and confirmed the stability of the triclinic structure to the range from 4 to 1073 K.

■ ASSOCIATED CONTENT

Supporting Information. Table of crystallographic data collection, agreement factors, and isotropic or equivalent atomic displacements ($Å^2$) of $CuWO_4$ at different temperatures and pressures (PDF); X-ray crystallographic files of the refined structures (CIF). This material is available free of charge via the Internet at http://pubs.acs.org.

■ AUTHOR INFORMATION

Corresponding Author
*E-mail: javier.ruiz-fuertes@uv.es.

■ ACKNOWLEDGMENT

Portions of this research were carried out at the light source DORIS III at DESY, a member of the Helmholtz Association (HGF). The authors thank HASYLAB for beamtime and European funding support through project II-20090231 EC. We thank the financial support from the MICINN of Spain under Grants No. MAT2007-65990-C03-03, MAT2010-21270-C04-01 and CSD2007-00045. We would also like to thank Martin Tolkiehn for assistance in using beamline D3. We thank SOLEIL for granting us beamtime and Alberta Congeduti for technical assistance at ODE beamline. J.R.-F thanks the MICINN for support through the FPI program as well as the European Commission within the European Light Sources Activities (ELISA) project. A.F. appreciates financial support from the Deutsche Forschungsgemeinschaft (Project FR2491-2 within SPP1236). W.M. acknowledges financial support from the BMBF, Germany (Project 05KS7RF1). The authors are grateful for the use of the SPP1236 central facility in Frankfurt.

■ REFERENCES

(1) Mikhailik, V. B.; Kraus, H. *Phys. Status Solidi (b)* **2010**, *247*, 1583–1599.
(2) Zhao, J.-H.; Liu, T.; Guo, S.-S.; Guan, J.; Wang, X. L. *Opt. Exp.* **2010**, *18*, 18989–18996.
(3) Li, C.-L.; Fu, Z. W. *Electrochim. Acta* **2008**, *53*, 4293–4301.
(4) Forsyth, J. B.; Wilkinson, C.; Zvyagin, A. I. J. *Phys.: Condens. Matter* **1991**, *3*, 8433–8440.
(5) Arora, S. K.; Mathew, T. *Phys. Status Solidi (a)* **1989**, *116*, 405–413.
(6) Bharati, R.; Shanker, R.; Singh, R. A. *Pramana* **1980**, *14*, 449–454.
(7) Lake, B.; Tennant, D. A.; Cowley, R. A.; Axe, J. D.; Chen, C. K. *J. Phys.: Condens. Matter* **1996**, *8*, 8613–8634.
(8) Kihlborg, L.; Gebert, E. *Acta Crystallogr., Sect. B* **1970**, *26*, 1020–1026.

(9) Ruiz-Fuertes, J.; Sanz-Ortiz, M. N.; González, J.; Rodríguez, F.; Segura, A.; Errandonea, D. J. *Phys. Conf. Series* **2010**, *215*, 012048.
(10) Ruiz-Fuertes, J.; Errandonea, D.; Lacomba-Perales, R.; Segura, A; González, J.; Rodríguez, F.; Manjón, F. J.; Ray, S.; Rodríguez-Hernández, P.; Muñoz, A.; Zhu, Z.; Tu, C.-Y. *Phys. Rev. B* **2010**, *81*, 224115.
(11) *CRYSALIS RED, version 171.31.5*; Oxford Diffraction: Wroclaw, Poland, 2006.
(12) Sheldrick, G. M. *Acta Crystallogr., Sect A* **2008**, *64*, 112–122.
(13) Boehler, R. *Rev. Sci. Instrum.* **2006**, *77*, 115103.
(14) Klotz, S.; Chervin, J.-C.; Munsch, P.; Le Marchand, G. J. *J. Phys. D: Appl. Phys.* **2009**, *42*, 075413.
(15) Finger, L. W.; King, H. E. *Am. Mineral.* **1978**, *63*, 337–342.
(16) Eichhorn, K. *REDUCE*; HASYLAB/DESY: Hamburg, Germany, 1987.
(17) Eichhorn, K. *AVSORT*; HASYLAB/DESY: Hamburg, Germany, 1978.
(18) Angel, R. J. J. *Appl. Crystallogr.* **2004**, *37*, 486–492.
(19) LeToullec, R.; Pinceaux, J. P.; Loubeyre, P. *High Pres. Res.* **1988**, *1*, 77–90.
(20) Schofield, P. F.; Redfern, S. A. T. J. *Phys. Chem. Solids* **1993**, *54*, 161–170.
(21) Sanz-Ortiz, M. N.; Rodríguez, F. J. *Chem. Phys.* **2009**, *131*, 124512.
(22) Ruiz-Fuertes, J.; Errandonea, D.; López-Moreno, S.; González, J.; Gomis, O.; Vilaplana, R.; Manjón, F. J.; Muñoz, A.; Rodríguez-Hernández, P.; Friedrich, A.; Tupitsyna, I. A.; Nagornaya, L. L. *Phys. Rev. B* **2011**, *83*, 214112.
(23) Hahn, D. *International Tables for Crystallography. Vol. A: Space-Group Symmetry*; D. Reidel Publishing Company: Dordrecht, The Netherlands, 1983.
(24) Ressler, T. J. J. *Synchrotron Radiat.* **1998**, *5*, 118–122.
(25) Rehr, J. J.; Albers, R. C. *Rev. Mod. Phys.* **2000**, *72*, 621–654.